doi:10.1016/S0022-2836(03)00238-9 *J. Mol. Biol.* (2003) **327**, 1121–1133

JMB

Available online at www.sciencedirect.com

SCIENCE DIRECT®

Quantitative NMR Studies of High Molecular Weight Proteins: Application to Domain Orientation and Ligand Binding in the 723 Residue Enzyme Malate Synthase G

Vitali Tugarinov and Lewis E. Kay*

Protein Engineering Network Centres of Excellence and the Departments of Medical Genetics Biochemistry and Chemistry University of Toronto 1 King's College Circle Toronto, Ont. Canada M5S 1A8

*Corresponding author

A high-resolution multidimensional NMR study of ligand-binding to *Escherichia coli* malate synthase G (MSG), a 723-residue monomeric enzyme (81.4 kDa), is presented. MSG catalyzes the condensation of glyoxylate with an acetyl group of acetyl-CoA, producing malate, an intermediate in the citric-acid cycle. We show that despite the size of the protein, important structural and dynamic information about the molecule can be obtained on a per-residue basis. $^{15}N-^{1}HN$ residual dipolar couplings and carbonyl chemical shift changes upon alignment in Pf1 phage establish that there are no significant domain reorientations in the molecule upon ligand binding, in contrast to what was anticipated on the basis of both the X-ray structure of the glyoxylate-bound form of the enzyme and structural studies of a related set of proteins. The chemical shift changes of ^{1}HN, ^{15}N and ^{13}CO nuclei upon binding of pyruvate, a glyoxylate-mimicking inhibitor, and acetyl-CoA have been mapped onto the three-dimensional structure of the molecule. Binding constants of pyruvate, glyoxylate, and acetyl-CoA (in the presence of pyruvate) have been measured, along with the kinetic parameters for glyoxylate and pyruvate binding. The on-rates of pyruvate and glyoxalate binding, $\sim 1.2 \times 10^6\ M^{-1}\ s^{-1}$ and $\sim 2.7 \times 10^6\ M^{-1}\ s^{-1}$, respectively, are significantly lower than what is anticipated from a simple diffusion-controlled process. Some structural implications of the chemical shift perturbations upon binding and the estimated ligand on-rates are discussed.

Keywords: ligand binding; malate synthase G; dipolar couplings; protein domains; multi-dimensional NMR

Introduction

Malate synthase G (MSG) from *Escherichia coli*, a 723-residue monomeric enzyme[1] (81.4 kDa), catalyzes the Claisen condensation of glyoxylate with an acetyl group of acetyl-CoA, as shown in Figure 1(a), producing malate, an intermediate in the citric-acid cycle. The reaction involves the inversion of configuration at the methyl group of acetyl-CoA, as with other Claisen enzymes such as citrate synthase.[2,3] The enzymatic abstraction of a proton from the α-methyl group of the acetyl CoA thio-ester, which is the rate-determining step, has long been considered to present both a kinetic and an energetic challenge for weak bases typically available in proteins[3] and has led to an interest in structural studies of this enzyme. Recently the crystal structure of MSG complexed with magnesium and glyoxylate was solved at 2.0 Å resolution.[4] MSG is a multi-domain enzyme, comprised of four main domains as illustrated in Figure 1(b). The centrally located core of the molecule is based on a highly stable β8/α8 barrel fold (residues 117–134, 263–295, 334–550). It is supported on one side by an N-terminal α-helical clasp (residues 3–88), which is linked to the first strand of the barrel by a long extended loop (residues 89–116). On the opposite side of the barrel is an α/β domain comprising residues 135–262 and a loop (residues 296–333) extending from the molecular core. The C-terminal end of the enzyme

Abbreviations used: MSG, malate synthase G; CSA, chemical shift anisotropy; HNCO, ^{1}H, ^{15}N, ^{13}CO 3D NMR correlation; TROSY, Transverse Relaxation Optimized Spectroscopy.

E-mail address of the corresponding author: kay@pound.med.utoronto.ca

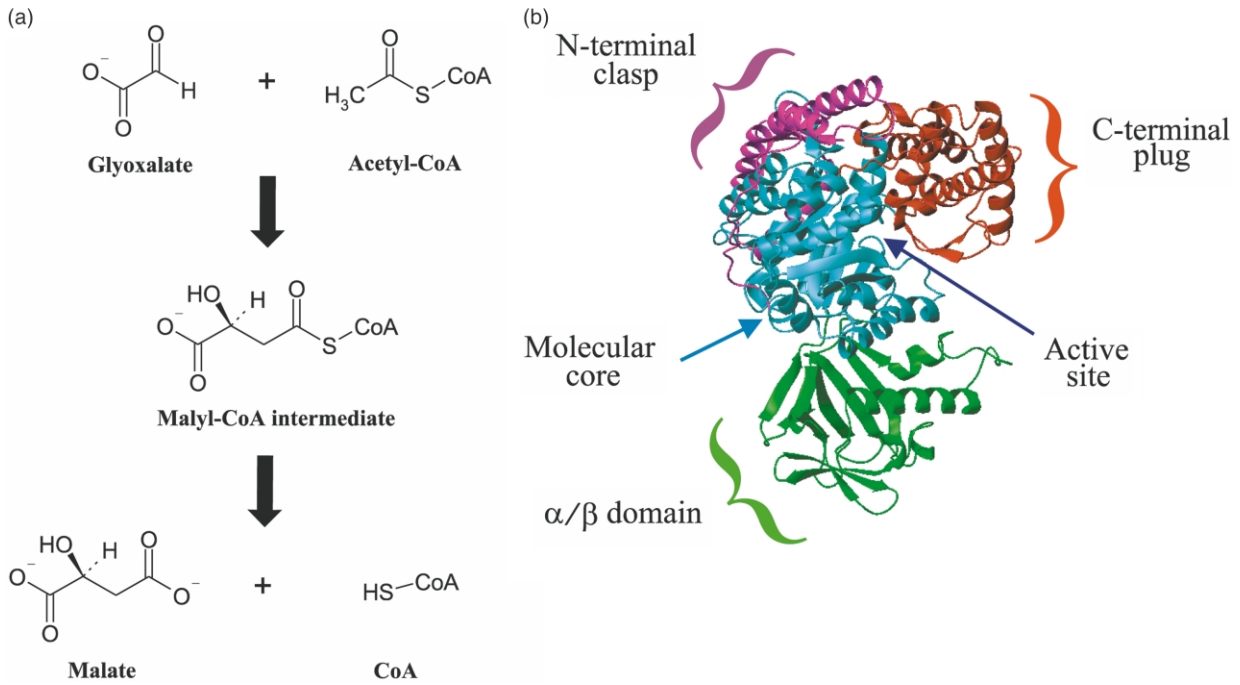

Figure 1. (a) Reaction catalyzed by malate synthase G. The reaction proceeds *via* a Claisen condensation of glyoxylate with the acetyl group of acetyl-CoA producing malate and CoA. (b) Ribbon diagram of MSG illustrating the four main domains of the molecule. The MSG coordinates were taken from the Protein Data Bank, accession code 1d8c[4].

(589–723) consists of a five-helix plug connected to the barrel by a flexible loop-helix-turn-helix-loop motif (residues 551–588). In addition, several smaller loops protrude from the globular core of the molecule. The active site of the enzyme is located in a cleft at the interface between the C-terminal plug and loops at the C-terminal ends of several of the β-strands of the core barrel. It was suggested based on the crystallographic data that the C-terminal plug may be mobile and that its position relative to the rest of the enzyme may be different in apo (open) and substrate-bound (closed) states of the molecule.[4] Such mobility would then facilitate opening of the active site cleft for substrate binding and product release. Earlier circular dichroism studies of substrate binding to both yeast and maize malate synthases indicated that significant conformational changes occur in the enzyme upon ligand binding.[5,6] Proteolysis studies with the maize enzyme support the notion of a flexible linkage between core and C-terminal domains that is rigidified upon acetyl-CoA binding.[6] Low-angle X-ray scattering studies on trimeric malate synthase from baker's yeast have shown that there is a decrease in the radius of gyration upon substrate binding.[7]

Domain reorientations are likely to occur in a number of other enzymes that are either structurally or mechanistically similar to MSG. Pyruvate kinase[8] (PK) is a close structural analog of MSG.[4] In PK the C-terminal extension is located opposite the active site but a large insertion within the sequence of the TIM-barrel core folds over the binding site and plays the role of the C-terminal plug in MSG. X-ray studies of PK with magnesium, potassium and L-phospholactate[9] establish that the protein is a tetramer with two tetramers per asymmetric unit. The inserted domain is observed in different positions relative to the TIM-barrel core in the different copies of the protein, with the transformation from the most "open" to the most "closed" copy given by a rotation of greater than 20°. This leads to significant differences in the degree of closure of the active site cleft between molecules.[9] Citrate synthase is a TCA cycle enzyme that catalyzes a very similar reaction to MSG but with a completely different fold.[4,10] Dimeric citrate synthase undergoes a large conformational change, in which the C-terminal domain rotates from the main body of the dimer by approximately 18° to open the active site for substrate entrance and product release.[10]

It is clear that in order to obtain a complete description of the catalytic mechanism of *E. coli* MSG it is of considerable importance to establish how the orientation of the domains in the protein change and what intra-domain structural perturbations occur in response to ligand binding (only the glyoxylate-bound structure of *E. coli* MSG is currently available). NMR is a particularly powerful probe of ligand-induced structural changes in macromolecules and related studies on a large number of diverse systems have been published over a period of many years. However, applications involving MSG are complicated by both the molecular weight (82 kDa) and the number of residues in the protein (723) and it was not clear *a priori* whether data of sufficient quality could be

obtained to allow us to address in a quantitative manner issues of domain orientation, as well as kinetic aspects of ligand binding. The demonstration that, in fact, such information can be obtained in this case is one of the major results of this study.

Building on the virtually complete backbone chemical shift assignments of apo-MSG obtained from four-dimensional NMR spectroscopy[11] we present here the results of a domain orientation study of MSG in the apo-state. Specifically, we show that the relative orientation of domains is consistent with the inter-domain structure of the glyoxylate-bound form of the protein observed by X-ray crystallography.[4] The absence of domain rearrangements upon ligand binding is distinct from what has been observed in versions of the protein isolated from other species[5–7] and in other very related molecules.[9,10] However, chemical shift changes upon pyruvate and acetyl-CoA binding to MSG and the kinetic parameters of glyoxylate and pyruvate binding extracted from line-shape simulations indicate that some minor structural perturbations are likely to take place upon formation of enzyme–substrate complexes.

Results and Discussion

Domain orientation in apo-MSG from residual dipolar couplings

The development of dilute liquid crystalline media for weak alignment of macromolecules[12–16] along with sensitive methods for the measurement of dipolar couplings resulting from alignment[17–20] have impacted significantly on the types of structural problems that can be addressed by NMR spectroscopy. One particularly important application involves measurement of orientational restraints to align domains of a molecule with respect to one another.[21,22] We have recently completed a dipolar coupling study of the ligand dependence of domain orientation in maltose binding protein, a 42 kDa single polypeptide chain comprised of two domains.[22,23] Notably, we find that in a complex with the cyclic hepta-saccharide β-cyclodextrin,[22] the relative orientation of the domains differs between solution and crystal conformations by 10°, while for other complexes and in the apo-form, the inter-domain structures obtained from NMR and X-ray analyses are very similar.[23]

The $^{15}N-^{1}HN$ dipolar coupling ($^{1}D_{NH}$) is by far the largest of those that can be measured in uniformly deuterated proteins and we have therefore chosen to obtain these values as a probe of domain orientation in MSG. However, the measurement of $^{1}D_{NH}$ in high molecular weight systems such as MSG is complicated by the fact that one of the two $^{15}N-^{1}HN$ multiplet components, referred to in what follows as the anti-TROSY component, is significantly broadened due to the constructive addition of dipolar and chemical shift anisotropy (CSA) fields.[24] Since the distance between the components must be obtained in any measurement of dipolar couplings, the accuracy of $^{1}D_{NH}$ values is limited by the broadening/intensity of the anti-TROSY cross-peak. With this in mind, Yang *et al.*[18] and Bax and co-workers[19] have developed TROSY-based HNCO experiments for measurement of $^{1}D_{NH}$ values (Figure 2(a)). $^{1}D_{NH}$ is obtained by recording a pair of spectra, the first of which is a simple reference TROSY-HNCO in which the observed correlation is the red peak in Figure 2(a). In a second experiment correlations at the position indicated by the blue peak are recorded,[18,19] so that the separation between cross-peaks in the set of two experiments is given by $(^{1}J_{NH} + {}^{1}D_{NH})/2$ Hz and the value of $^{1}D_{NH}$ is readily obtained once the scalar coupling, $^{1}J_{NH}$, is known (see below). In principle, it is possible to modify the second experiment so that correlations at any position between the red (TROSY) and green (anti-TROSY) peaks in the Figure can be obtained. At first glance it might appear, therefore, that positioning cross-peaks as far from the red correlation as possible in the second experiment would be desirable to minimize the resultant error in $^{1}D_{NH}$ values. However, because the effective relaxation rate of signal increases as the position of the cross-peak shifts towards the green correlation, a compromise must be made between a large separation of components in the two experiments on the one hand and sufficient sensitivity to measure the correlations accurately in the first place. We have confirmed experimentally that the choice of scaling used in the present set of experiments is optimal for MSG.

In Figure 2(a) we have also included average ^{15}N transverse relaxation rates for the TROSY (~65 ms) and anti-TROSY (~10 ms) multiplet components measured on a deuterated sample of MSG, as described previously.[11] In addition, the average T_2 value for in-phase ^{15}N magnetization (recorded with ^{1}H decoupling to inter-convert TROSY and anti-TROSY components) is shown. These values provide a qualitative indication of the dramatic increase in relaxation rates that can be expected for non-TROSY magnetization in a protein the size of MSG. A more quantitative estimate, taking into account the specific details of the pulse sequence and the experimental parameters employed, shows that the effective relaxation time of ^{15}N magnetization that gives rise to the "blue correlations" in Figure 2 is approximately 30 ms.

Figure 2(b) shows cross-peaks obtained in reference HNCO (red) and coupling-refocused HNCO (blue) spectra for Gly414 and Ala541 recorded on a sample of MSG dissolved in ~12 mg/ml Pf1 phage. It is noteworthy that the up-field peaks in Figure 2(b) are significantly broader than the downfield (reference TROSY) peaks, as expected from the above discussion. The large size of the protein, coupled with the fact that the sample used was relatively dilute (0.7 mM) and that the measured coupling values are halved in the

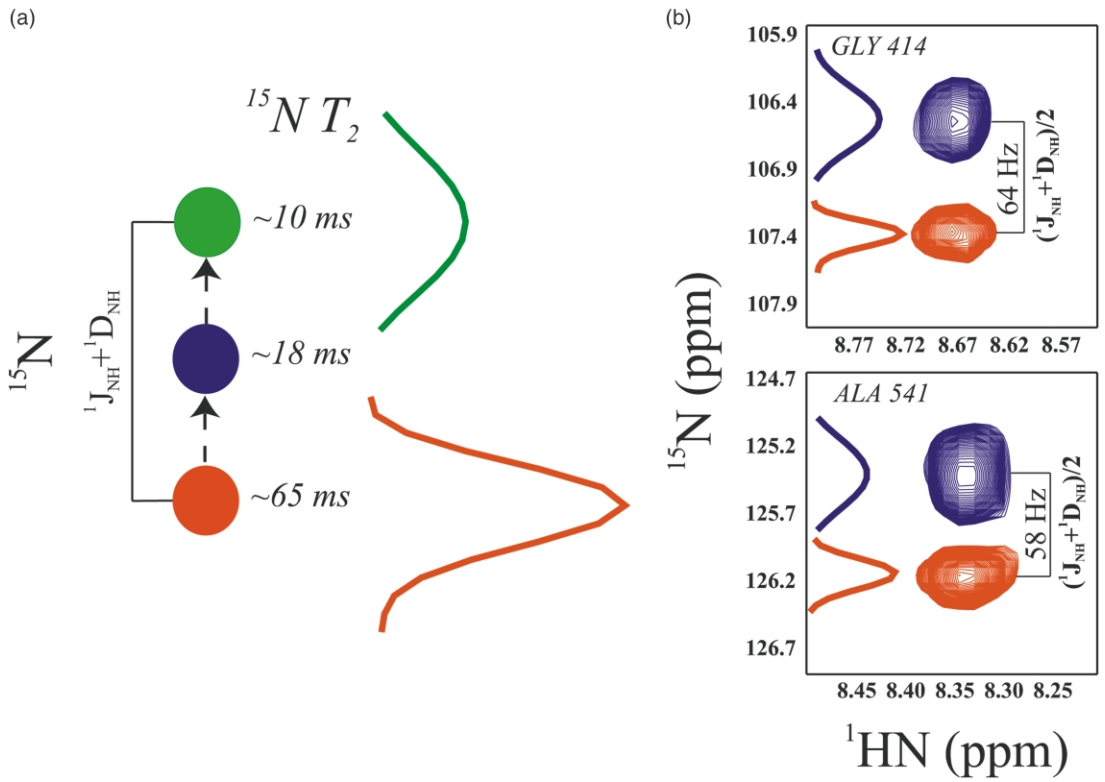

Figure 2. (a) A schematic illustration of the positions of the TROSY (red), decoupled (blue) and anti-TROSY (green) ^{15}N multiplet components. In order to measure $^1J_{NH}$ or $^1J_{NH} + {}^1D_{NH}$ values two spectra are recorded, producing correlations of the "red" and "blue" types. Average ^{15}N T_2 relaxation times for each component are indicated; the ^{15}N T_2 value of the anti-TROSY component was estimated from the measured relaxation rates of ^1H-decoupled and TROSY components. (b) Correlations for G414 and A541. Note that the upfield and downfield cross-peaks are derived from separate spectra, as discussed in Results and Discussion, and have been combined here for ease of visualization. The splittings are equal to $(^1J_{NH} + {}^1D_{NH})/2$.

procedure that we have employed, does significantly increase the errors relative to what is generally observed for applications involving smaller molecules. For example, the standard error of the measured $^1J_{NH}$ values estimated on the basis of duplicate experiments is 2.0 Hz, in excellent agreement with the standard deviation of the coupling values, 1.99 Hz. Of note, contributions to $^1J_{NH}$ from magnetic susceptibility anisotropy, estimated by calculating a susceptibility tensor from the orientation of aromatic rings and peptide bonds in the molecule,[25–27] range from +1.1 Hz to −0.9 Hz (800 MHz), with a standard deviation of 0.48 Hz. The standard error of the $(^1J_{NH} + {}^1D_{NH})$ measurements in the aligned phase as estimated from duplicate experiments is 2.7 Hz, reflecting the somewhat lower quality of NMR spectra obtained for MSG aligned in Pf1 phage.[13]

A total of 415 $^1D_{NH}$ couplings, ranging between −40 Hz and +35 Hz have been obtained by (i) subtracting the experimentally determined $^1J_{NH}$ values from the measured $^1J_{NH} + {}^1D_{NH}$ values, as is commonly done,[12] and (ii) by subtracting an average $^1J_{NH}$ value of −93.9 Hz from $^1J_{NH} + {}^1D_{NH}$. Residues with significantly higher than average ^{15}N $T_{1\rho}$ values,[11] or correlations that were partially overlapped were excluded from analysis. In addition, a small number (22) of $^1D_{NH}$ values were excluded because differences in dipolar couplings larger than 4.5 Hz were obtained from repeat measurements. Since the relative orientation of different domains in the apo-form of MSG was not known *a priori*, the magnitude and orientation of alignment tensors were calculated separately for each individual domain assuming that the intra-domain structure in solution is the same as in the glyoxylate-bound form determined by X-ray studies.[4] The alignment tensor parameters, A_a and R, and the Euler angles, {α, β, γ} that define the orientation of each alignment frame with respect to the PDB frame of the molecule are shown in Figure 3(a)–(d), along with the correlation between measured dipolar couplings and those calculated on the basis of the domain structures. In this Figure we have used $^1D_{NH}$ values obtained assuming a uniform $^1J_{NH}$ value of −93.9 Hz (see above), although very similar results are generated using measured scalar couplings. The agreement between calculated and experimental coupling values is very good, especially considering the errors in the measurement. Compatibility between the dipolar coupling set and the X-ray structure

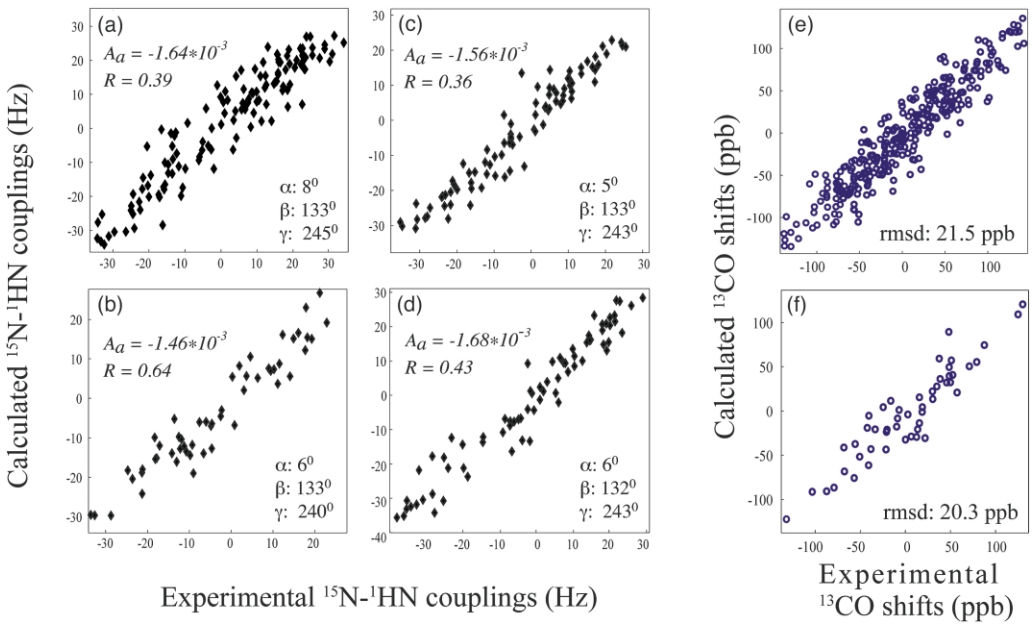

Figure 3. Experimental *versus* calculated $^1D_{NH}$ values for the (a) core domain (136 values), (b) N-terminal α-clasp (55 values), (c) α/β domain (89 values), and (d) C-terminal plug (73 values). The values of Euler angles and the magnitudes of the alignment parameters, A_a, R obtained for each domain are indicated. Errors in {A_a, R, α, β, γ} of {0.03×10^{-3}, 0.02, 1.1°, 0.5°, 1.4°}, {0.09×0^{-3}, 0.13, 6.5°, 1.5°, 3.9°}, {0.04×10^{-3}, 0.03, 1.2°, 0.6°, 2.3°} and {0.04×10^{-3}, 0.04, 1.4°, 0.7°, 2.4°} are obtained for the core, N-terminal, α/β and C-terminal domains, respectively. Experimental *versus* calculated carbonyl shifts upon alignment of MSG in Pf1 phage for (e) the whole molecule and for (f) residues of the C-terminal plug. The alignment tensor obtained from the full set of $^1D_{NH}$ data was used for the calculation of ^{13}CO shifts.

of glyoxylate-bound MSG was established in a quantitative manner by calculating quality factors (Q):

$$Q = \sqrt{\frac{\sum_{i=1,N} (D_i^{meas} - D_i^{calc})^2}{\sum_{i=1,N} (D_i^{meas})^2}} \quad (1)$$

as defined by Ottiger & Bax.[15] Quality factors of 0.32, 0.27, 0.25, and 0.24 were obtained for the MSG core, the α-helical N-terminal clasp, the α/β domain, and the C-terminal plug, respectively. The magnitudes of the alignment tensor are well reproduced from one domain to another. The slightly lower (absolute) value of the axial component of the alignment tensor (A_a) and the higher rhombicity (R) in the N-terminal clasp may be the result of a skewed sampling of N–H bond vector orientations in this part of the protein since this domain consists primarily of a single long α-helix.[4] Very similar values of the three Euler angles were obtained for all the domains of MSG indicating that, contrary to the predictions based on earlier studies with *E. coli* MSG[4] and related proteins,[7,9,10] the domain orientations in the apo-form are not significantly different from those found in the glyoxylate-bound form. Thus, the gross features of the active site within the crevice between C-terminal and core domains are preformed in the apo-state and subtle structural changes likely involving side-chains dominate substrate binding. In principle, a translational displacement of the C-terminal plug would not be reflected in the values of $^1D_{NH}$ and therefore cannot be ruled out. However, such translational movements would be very unlikely in the case of MSG where the contact surface area between the molecular core and the C-terminal plug is close to 2000 Å^2, since it would lead to the disruption of numerous inter-domain interactions.[4]

Carbonyl chemical shift changes upon alignment

Changes in chemical shifts upon alignment can also provide valuable structural information[28–30] and have been used to orient domains of proteins[31] and in the refinement of protein[32] and nucleic acid structures.[33] The carbonyl chemical shift is a particularly good probe of structure[29] since the shift anisotropy of the carbonyl nucleus is large[34] and because shifts can be measured accurately using TROSY-based HNCO spectra.[35,36] In this case it is advantageous to record spectra at fields of 600 MHz or lower, because the relaxation of the carbonyl spin is dominated by CSA, which scales with the square of the magnetic field. For example, at 800 MHz the calculated contribution to the relaxation rate of a carbonyl spin in MSG (37 ns correlation time at 37 °C) from CSA is 93 s^{-1} (corresponding to a T_2 of 10.8 ms), which compromises the accuracy with which such chemical shifts can be measured. A total of 320 carbonyl shifts were

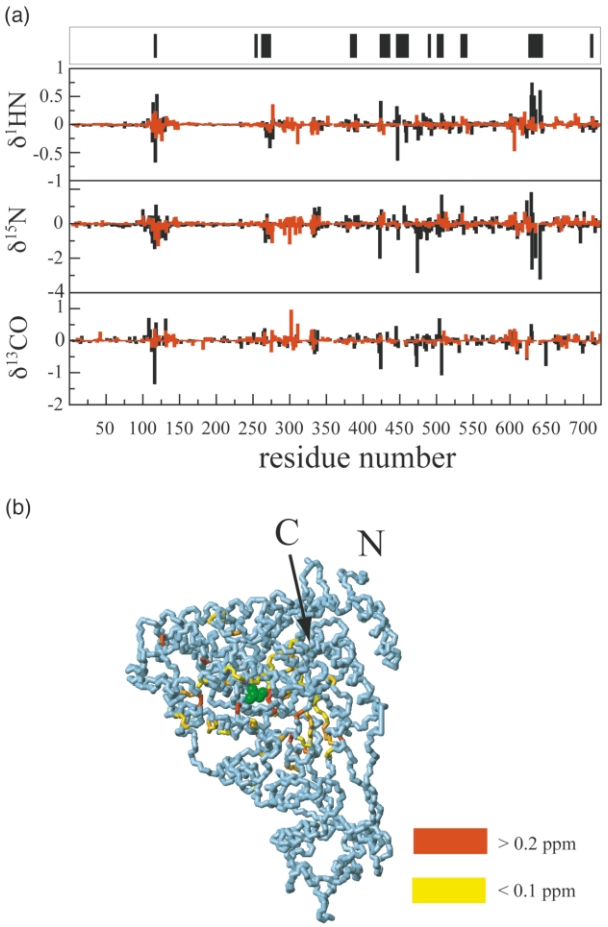

Figure 4. (a) ^{1}HN, ^{15}N and ^{13}CO chemical shift changes in MSG upon binding of pyruvate (black) and acetyl-CoA after saturation with pyruvate (red) *versus* residue number. The residues of MSG with atoms closer than 8 Å to any of the heavy atoms of the bound glyoxylate in the MSG crystal structure[4] are shown in black above the plot. (b) Combined chemical shift changes[37] upon binding of pyruvate color-coded onto the 3D structure of MSG (PDB accession code 1d8c[4]). The shift changes shown in red exceed 0.2 ppm and those shown in yellow are >0.04 ppm and <0.1 ppm. A gradient of color is used to indicate shift changes between 0.1 ppm and 0.2 ppm. The bound glyoxylate molecule is shown in green. The Figure was prepared with the program MOLMOL.[56]

obtained for MSG from 3D TROSY-HNCO spectra recorded at 600 MHz. Figure 3(e) shows the excellent agreement between all experimentally measured values and those calculated from X-ray coordinates of the MSG–glyoxylate complex[4] using the orientation and magnitude of the alignment tensor obtained from the full set of ^{15}N–^{1}HN dipolar couplings. The correlation of shifts obtained for the C-terminal plug domain of MSG exclusively is shown in Figure 3(f), and again very good agreement is observed. Of note, the level of agreement between predicted and experimentally observed carbonyl shift changes upon alignment is only slightly worse than that obtained for measured and predicted ^{15}N–^{1}HN dipolar couplings (i.e. similar Q factors) even though the absolute values of the shift differences are significantly less than peak line widths in the carbonyl dimension of TROSY-HNCO spectra.

The carbonyl shift changes are fully consistent with the lack of domain rearrangement upon ligand binding indicated by the dipolar coupling data. Very recently, Remington and co-workers have obtained preliminary structures of apo and pyruvate/acetyl-CoA-bound forms of MSG (personal communication) that show that there are no major structural differences between any forms of the protein, in agreement with the results of the present study.

Ligand-induced chemical shift changes in MSG

In order to probe possible minor structural changes that occur with ligand binding we have measured chemical shift changes that accompany the titration of apo-MSG with pyruvate. Pyruvate serves as an inhibitor that competes with the natural substrate glyoxylate in binding to the active site of the protein, and can be used in place of glyoxylate to form a stable ternary (MSG-pyruvate/acetyl-CoA) complex (note that glyoxylate is converted to malate in an MSG glyoxylate/acetyl-CoA complex). Since 2D ^{1}HN–^{15}N correlation maps of MSG are not sufficiently resolved, 3D TROSY-HNCO spectra were used to follow 3D trajectories of the resonances experiencing chemical shift changes upon pyruvate binding. Notably, the chemical shift changes were predominantly small and localized to several stretches in the MSG sequence, so that unambiguous assignments of nearly all those amides assigned in the apo-form were possible (98.6%). After the enzyme was saturated with pyruvate the sample was titrated with acetyl-CoA, and the assignment procedure was repeated. A total of 95.5% of all the amides assigned in the apo-form were available for analysis in the pyruvate/acetyl-CoA-bound form. Unfortunately, several residues belonging to the active site could not be identified since they were unassigned in the apo-form of the protein.[11] Figure 4(a) summarizes the chemical shift changes upon pyruvate (black) and pyruvate/acetyl-CoA (red) binding. Relative to changes in chemical shifts observed in a ligand binding study involving maltose-binding protein,[23] the shift changes noted upon pyruvate binding to MSG are quite small, with maximal changes in the ^{1}HN, ^{15}N, and ^{13}CO dimensions of 0.74 (E630), 3.2 (H641), and 1.3 ppm (Q116), respectively. Notably, the most significant changes in ^{15}N and ^{1}HN chemical shifts upon pyruvate binding occur in the I615-H641 stretch. Most of this region in MSG is part of the β-hairpin loop in the C-terminal domain that interfaces with the TIM core barrel.[4] The observed shifts indicate that some minor structural changes in this region accompany the binding of pyruvate.

Despite the aromatic moiety of acetyl-CoA, its binding results in shift perturbations that are on

average 2.0–2.5 times smaller than what is noted upon pyruvate binding. These shifts are, in general, confined to the same regions in the protein sequence that are observed for pyruvate binding, with the addition of significant changes in the 300–310 flexible loop in the acetyl-CoA-bound form. In addition, a 2D ^{1}HN–^{15}N correlation-based titration of apo-MSG with glyoxylate was carried out to get (limited) information about changes that accompany glyoxylate binding. Of the approximately 200 correlations in the 2D spectra that were sufficiently well resolved to be quantified, 32 peaks showed measurable shift changes that were, in general, somewhat larger in absolute value than those occurring upon pyruvate binding. All shift changes were in the same direction as noted for pyruvate with the exception of the amide ^{15}N and ^{1}HN shifts of W509. The amide proton and nitrogen atoms of W509 are 9.7 Å and 9.5 Å away from the aldehyde carbon of glyoxylate in the MSG crystal structure,[4] respectively, and are therefore likely to be in proximity to the methyl group of pyruvate in the pyruvate-MSG complex.

Figure 4(b) displays the combined ^{15}N and ^{13}C backbone chemical shift changes[23,37] (see Materials and Methods) that occur upon pyruvate binding color-coded onto the crystal structure of glyoxylate-bound MSG.[4] Though the ligand-induced changes are clearly spatially concentrated around the glyoxylate-binding site, several residues with significant shift changes are almost 20 Å away from the glyoxylate molecule. For example, the chemical shifts in the loop spanning residues 89–115 linking the N-terminal clasp with the molecular core consistently changed in all of the titration series. Only the side-chain atoms of V118 and the carboxyl group of E116 within this loop are within 10 Å of the bound glyoxylate. These changes may be indicative of minor conformational changes in the interface between the molecular core and the N-terminal α-helix that are necessary to accommodate the substrate in the active site. No significant chemical shift changes were observed for the residues linking the core of the molecule with the C-terminal plug (551–589). In sum, the titration data provide evidence that major structural rearrangements do not accompany ligand binding in MSG, consistent with the results of the dipolar coupling study and carbonyl shift changes that occur upon alignment described above.

Relaxation and hydrogen exchange measurements support the absence of significant structural changes upon ligand binding

It was shown in our previous study that apo-MSG tumbles as a single spherical particle with a correlation time of 37 ns at 37 °C.[11] We have supplemented the ^{15}N relaxation study of apo-MSG described previously by recording ^{15}N $T_{1\rho}$ values for the protein in the pyruvate and pyruvate/acetyl-CoA-bound states and these values along with those for the free form of the enzyme are plotted as a function of residue number in Figure 5(a). The same subsets of 165 well resolved peaks in 2D ^{1}HN–^{15}N correlation maps of MSG were selected for each state of the protein for the comparison. The relaxation times were found to be homogeneous and small (~20 ms) throughout the MSG sequence for all forms of the protein, except for several residues in flexible loops, including the loop comprising residues 143–160 in the α/β domain, the 300–310 flexible stretch that is missing from the X-ray coordinates of MSG,[4] and the linker between the molecular core and the C-terminal plug. Of note, the 300–310 loop appears to be more rigid in the pyruvate/acetyl-CoA-bound state, reflected in the lower ^{15}N $T_{1\rho}$ values in relation to the other forms of the protein.

The ^{15}N spin relaxation experiments described above probe dynamics on a ps-ns time scale. In order to establish whether there are slower processes that might be present we have also measured hydrogen exchange with solvent using 3D TROSY-HNCO versions of the CLEANEX-HSQC experiment.[38] The exchange rates of 28 amides could be quantified accurately (rates greater than ~3 s^{-1}) and are shown in Figure 5(b) for the apo-state of MSG. In general, regions with high exchange rates correlate well with those having elevated ^{15}N transverse relaxation times. Of note, a very similar exchange profile is obtained for the pyruvate bound state of the protein.

Kinetic parameters of ligand binding to MSG and structural implications

The binding of both pyruvate and glyoxylate to MSG occurs in the intermediate exchange regime on the NMR chemical shift time scale for many residues in the protein and it is therefore possible to quantify the kinetic parameters describing ligand binding in a straightforward manner. Figure 6(a) summarizes the results of a titration of apo-MSG (black) with pyruvate (fully bound is red), focusing on the well resolved region of the ^{1}HN–^{15}N HSQC-TROSY spectrum of the protein. In many cases considerable line-broadening is apparent at intermediate ligand concentrations. Equilibrium dissociation constants (K_d) of the glyoxylate, pyruvate and pyruvate/acetylCoA-MSG complexes were determined by least-squares fitting of the chemical shift changes accompanying ligand binding as a function of the total ligand concentration as described in Materials and Methods. The best-fit curves in both ^{15}N and ^{1}HN dimensions for V620 titrated with pyruvate and glyoxylate are shown in Figure 6(b) and (c), respectively. Estimated K_d values averaged over 20 well resolved peaks with significant shifts in either ^{1}HN or ^{15}N dimensions are 1.02(±0.15) mM and 600(±70) μM for pyruvate and glyoxylate, respectively. Notably, glyoxylate, the physiological

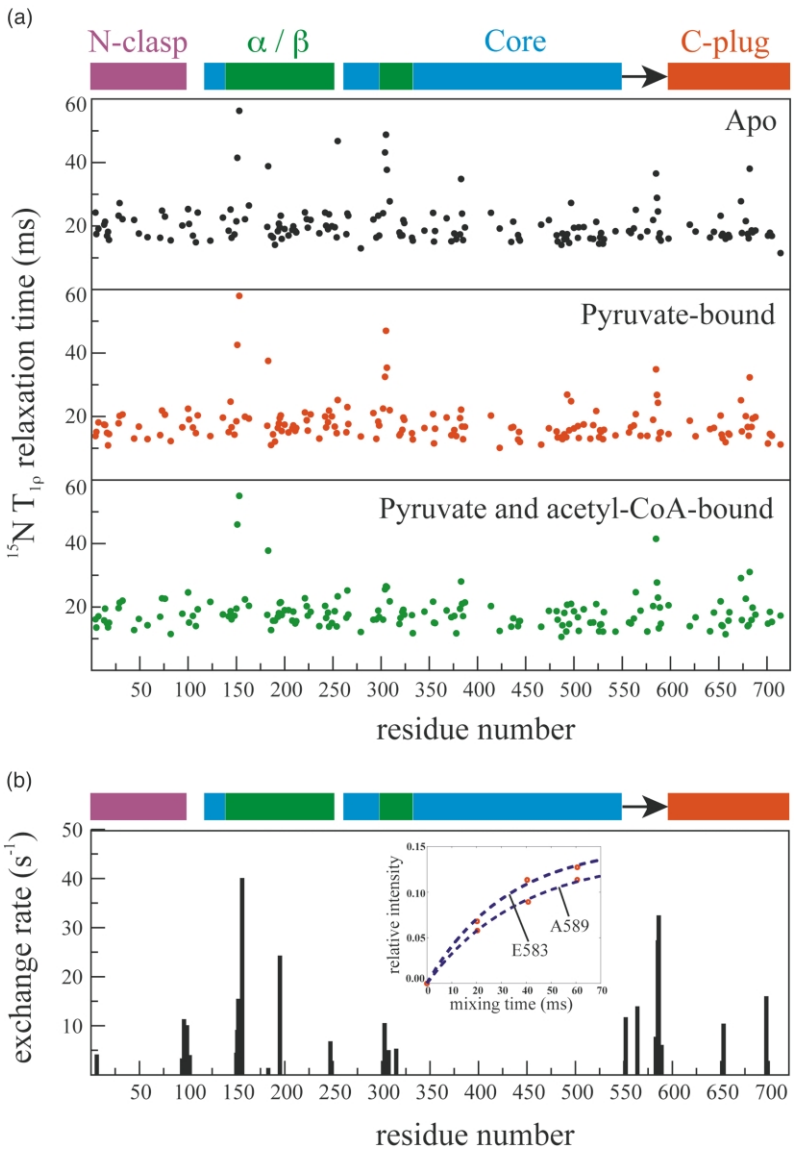

Figure 5. (a) ^{15}N $T_{1\rho}$ relaxation times *versus* the MSG sequence for the same subset of 165 well resolved residues in 2D TROSY-HSQC spectra of MSG in the apo (black), pyruvate-bound (red) and pyruvate/acetyl-CoA-bound (green) protein states. (b) Solvent exchange rates for the amides of apo-MSG *versus* residue number. The inset shows the build-up of peak intensities for residues E583 and A589 as a function of mixing time. Regions corresponding to the different domains of MSG are color coded above the plots.

substrate of MSG, binds more strongly than pyruvate. The K_d value for acetyl-CoA binding to the pyruvate-saturated form of MSG could not be determined with the same degree of accuracy as the other ligands because of generally smaller shift changes and was estimated as 270($\pm$120) μM.

The exchange kinetics of binding have been determined for both pyruvate and glyoxylate assuming that the binding reaction can be described in its simplest form as:

$$P + L \underset{k_{off}}{\overset{k_{on}}{\leftrightarrow}} PL \qquad (2)$$

where P, L and PL denote free protein, free ligand and complex, respectively. NMR line broadening is a function of k_{on}[L] and k_{off} and is, therefore, an excellent probe of exchange kinetics.[39] A number of different methods have been used in the past to measure binding kinetics including relaxation dispersion spectroscopy[39] and line-shape analysis.[40–42] Here we have used the latter approach by curve-fitting the line-shapes derived from 2D ^{1}HN–^{15}N TROSY-HSQC spectra recorded at different ligand concentrations. Since the dissociation constants ($K_d = k_{off}/k_{on}$) are already known a series of N spectra belonging to the same titration set can be fit to a common on-rate, k_{on}, and a set of N constants that scale each of the spectra independently. These constants account for the fact that in any given fitting only a single dimension of a 2D spectrum is considered; any change in line width in the second (unfitted) dimension that occurs upon ligand binding also influences the intensity of peaks.[42] Second, the efficiency of magnetization transfer during constant-time periods in the 2D experiment will be a function of the relaxation properties of both ^{1}HN and ^{15}N magnetization, which will change with added ligand. Figure 6(d) and (e) shows the two best examples of line-shape simulations from titration data for glyoxylate (^{1}HN dimension of I482) and pyruvate (^{15}N

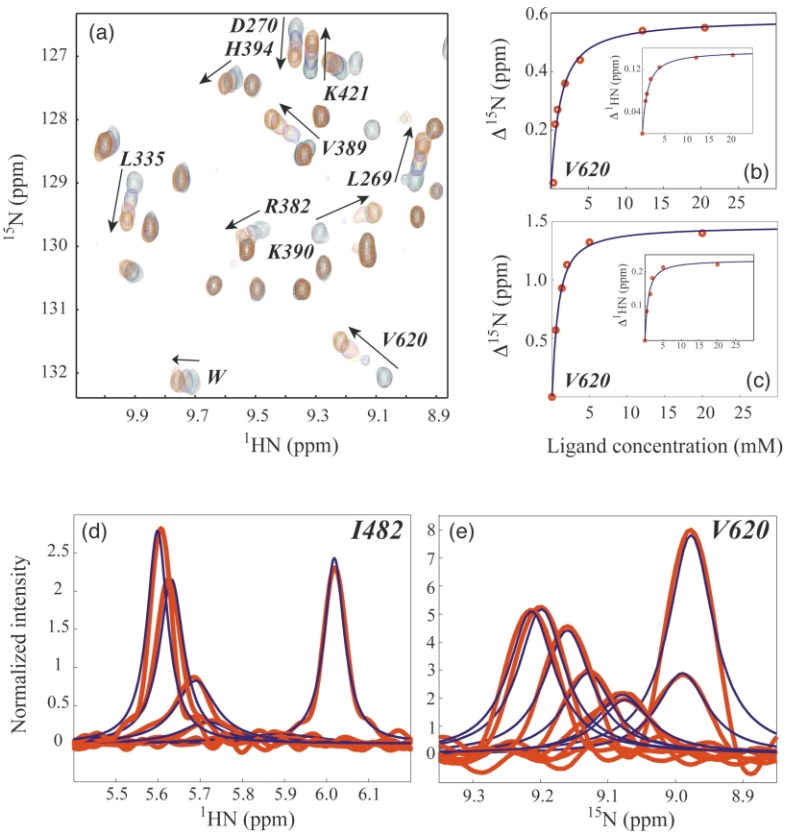

Figure 6. (a) Overlay of a selected region of 800 MHz ^{1}HN–^{15}N TROSY-HSQC spectra of [^{15}N, ^{2}H]-labeled MSG recorded as a function of pyruvate concentration. Arrows indicate the directions of peak movement. Resonances with significant chemical shift changes are labeled with residue numbers. (b) and (c) K_d determination using chemical shift changes of V620 upon titration with (b) pyruvate and (c) glyoxylate. The insets show the best-fits from changes in ^{1}HN shifts. (d) and (e) Examples of line-shape simulations for (d) I482 (^{1}HN dimension) in titration with glyoxylate and (e) V620 (^{15}N dimension) in titration with pyruvate. Experimental line-shapes are shown in red and the results of the simulations are shown in blue.

dimension of V620), respectively. It is noteworthy that even in the cases where the chemical shift changes in only one dimension (e.g. the ^{15}N chemical shift of I482 does not change upon titration with glyoxylate) severe signal attenuation may occur at intermediate ligand concentrations because of the much lower efficiency of INEPT magnetization transfers in the TROSY-HSQC spectra (see above).

The on-rates for pyruvate derived from line-shape fitting of five peaks in both dimensions vary between $0.8 \times 10^6\ M^{-1}\ s^{-1}$ and $1.5 \times 10^6\ M^{-1}\ s^{-1}$, while those for glyoxylate, derived from fitting four peaks in both dimensions, are slightly higher, 1.5×10^6–$3.8 \times 10^6\ M^{-1}\ s^{-1}$. These on-rates are about two orders of magnitude lower than bimolecular diffusion-controlled rates ($\sim 10^8$–$10^9\ M^{-1}\ s^{-1}$) and are similar to values reported for many enzymes and their substrates[43] (10^6–$10^8\ M^{-1}\ s^{-1}$). The entry rate of these ligands may be limited by the fact that they are polar and that binding is preceded by desolvation of the polar carboxylic group. Alternatively, there may be activation barriers associated with ligand burial inside the protein that are due to the polarity of the ligand or that reflect subtle structural rearrangements that occur upon binding. The latter interpretation is consistent with the large number of small chemical shift changes that are observed upon ligand binding. Of interest, the on-rates reported here are similar to those measured for the binding of benzene derivatives to the Leu99Ala cavity mutant of T4 lysozyme. It was suggested that in the lysozyme case the magnitude of these values may reflect more issues of charge burial/desolvation rather than steric constraints that must first be removed by dynamics.[44]

Conclusions

A major result of this study is that quantitative, site-specific structural and dynamic information can be obtained on systems as large as MSG. The present work has exploited recent developments in NMR methodology including the measurement of orientational restraints in partially aligned samples,[45] and the preservation of magnetization using the TROSY principle.[24] The latter is quite essential for applications involving molecules the size of MSG.

Based on dipolar couplings and chemical shift changes upon alignment it is clear that the inter-domain structures of the apo and glyoxylate-bound forms of MSG are very similar and that the changes expected on the basis of earlier work[4] do not occur. However, chemical shift changes upon pyruvate and acetyl-CoA binding to MSG and the kinetic parameters of glyoxylate and pyruvate binding extracted from line-shape simulations derived from titration data indicate that some minor structural adjustments are likely to take place upon formation of complexes. It is anticipated that multi-dimensional NMR will play an increasingly important role in the characterization

of the structural and dynamic features of large proteins at a level of quantification that until recently was reserved for only small molecular weight systems.

Materials and Methods

NMR samples

U-[^{15}N,^{13}C,^{2}H] and U-[^{15}N,^{2}H]-labeled samples of MSG were obtained by overexpression from cultures of *E. coli* BL21(DE3)pLysS cells transformed with the plasmid pMSG-B encoding all the residues of MSG with (i) the substitution of Ser2 with an Ala, (ii) the addition of an N-terminal Met and (iii) the addition of an eight-residue C-terminal hexa-histidine tag (LEHHHHHH) as described in detail.[11] For the preparation of ^{13}C-labeled samples [^{13}C,^{1}H]glucose (Cambridge Isotope Laboratories, Andover, MA) was used as the sole carbon source. After initial purification on a nickel affinity column (Ni-NTA Agarose, Qiagen) the protein was fully denatured and refolded *in vitro* in order to fully protonate the amide positions of those residues buried in the core of the molecule (and therefore deuterated after growths in the $^{2}H_2O$-based bacterial medium). The details of the *in vitro* refolding protocol and subsequent purification steps have been described.[11] The sodium salts of pyruvic and glyoxylic acids and acetyl-CoenzymeA used in the titrations described above were purchased from Sigma (Ontario, Canada) and were not further purified.

All NMR samples were between 0.3 mM and 0.8 mM in protein dissolved in 20 mM sodium phosphate buffer (pH 7.1), 5 mM DTT, 20 mM $MgCl_2$, 0.05% NaN_3, 0.1 mg/ml Pefabloc and 8% $^{2}H_2O$. Alignment of protein was achieved using a sample with Pf1 phage[13,46] added to a concentration of ~12 mg/ml (residual ^{2}H water splitting of 9.8 Hz), which provided ^{15}N–^{1}HN dipolar couplings between −40 Hz and +35 Hz.

NMR spectroscopy

All NMR experiments were performed on four-channel Varian Inova spectrometers operating at 37 °C and equipped with pulsed-field gradient triple resonance probes.

$^{1}D_{NH}$ values were measured for apo-MSG from 3D TROSY-HNCO-based spectra[18,19] recorded at 800 MHz. Two spectra were recorded in an interleaved manner, including a regular TROSY-HNCO and a TROSY-HNCO modified by including a ^{1}H inversion pulse at time $t/2$ prior to the end of the final ^{15}N constant-time evolution period, where t is the ^{15}N acquisition time.[18,19] The separation of cross-peaks in the pair of spectra is given by $(^{1}J_{NH} + {}^{1}D_{NH})/2$ Hz. Data sets comprised of $28 \times 54 \times 863$ complex points in each of t_1(^{13}CO), t_2(^{15}N), t_3(^{1}HN), corresponding to acquisition times of 13.4 ms, 23.4 ms and 68 ms were recorded, with eight (TROSY-HNCO) and 12 (TROSY-HNCO + ^{1}H inversion pulse) scans per FID (1.7 second relaxation delay) for a total acquisition time of approximately 60 hours per pair of experiments. Spectra were analyzed using PIPP/CAPP[47] software with uncertainties in $^{1}J_{NH}$ and $^{1}D_{NH}$ values obtained from the pair-wise r.m.s.d of coupling data in repeat experiments performed in both isotropic and aligned media (standard error in each of the two repeat experiments = $1/\sqrt{2}$ of the pair-wise r.m.s.d). 3D TROSY-HNCO[35,36,48] data sets were used to quantify the changes in carbonyl chemical shifts upon alignment, as described by Choy *et al.*[31] Data sets were recorded at 600 MHz and comprised $48 \times 54 \times 612$ complex points in t_1,t_2,t_3 (acquisition times of 31.2 ms, 31.2 ms, 64 ms in t_1,t_2,t_3). Eight scans were obtained per FID with a relaxation delay of 1.9 seconds to give a net measuring time of 44 hours for each data set. Selection of the TROSY component in all the experiments was achieved passively by relying exclusively on the efficient relaxation of the anti-TROSY component during the relatively long transfer delays in the pulse schemes.[35,49] All NMR spectra were processed using the suite of programs provided in NMRPipe/NMRDraw software.[50]

^{1}HN, ^{15}N and ^{13}CO chemical shift changes in MSG resulting from either pyruvate or acetyl-CoA binding were quantified by addition of aliquots of ligands and following peak trajectories in 3D TROSY-HNCO spectra recorded at 800 MHz. Pyruvate was added to a 0.35 mM U-[^{15}N,^{13}C,^{2}H]-labeled sample of MSG to give final ligand concentrations of 0.35, 0.72, 0.90, 1.90, 3.90, 12.2 and 20.5 mM; acetyl-CoA was subsequently added to the same sample to concentrations of 0.3, 0.7, 1.7 and 4.0 mM. Glyoxylate was added to a 0.50 mM U-[^{15}N,^{2}H]-labeled protein sample to give ligand concentrations of 0.5, 1.5, 2.0, 5.0 and 20.0 mM and the titration was monitored using a series of 2D TROSY-HSQC spectra. All spectra were analyzed using NMRView software[51] in conjunction with auxiliary tcl/tk scripts written in-house. The combined chemical shift change of a particular residue upon ligand binding was calculated as:

$$\Delta\delta_{tot} = \sqrt{(w_N \Delta\delta_N)^2 + (w_{CO} \Delta\delta_{CO})^2} \qquad (3)$$

where w_i denotes the weight factor of nucleus i. The weight factors were determined from the ratio of the average standard deviations of the ^{1}HN shifts and the chemical shifts of nucleus type i as observed for the 20 common amino acids in proteins using the BioMagResBank chemical shift database†: $w_{HN} = 1$, $w_N = 0.154$, and $w_{CO} = 0.341$.[23,37] ^{1}HN shifts were not taken into account in the calculation since proton shifts are more sensitive to neighboring effects than ^{13}C and ^{15}N chemical shifts. The value of $\Delta\delta_{tot}$ principally reflects, therefore, changes in backbone ϕ/ψ dihedral angles.

NMR experiments for the measurement of ^{15}N $T_{1\rho}$ at 800 MHz ^{1}H frequency made use of TROSY versions of pulse sequences described elsewhere.[52] The spin lock power used in the ^{15}N $T_{1\rho}$ experiments was 1.6 kHz. $T_{1\rho}$ values were determined by non-linear least-squares fitting of the experimental data to monoexponential decay functions, $A\exp(-t/T_{1\rho})$, using the program ModelXY[50] or MATLAB v.6 (MathWorks Inc., MA).

Amide hydrogen exchange rates with solvent were measured using a 3D TROSY-HNCO version of the CLEANEX experiment[38] with exchange times of 22, 44 and 66 ms. Spectra were recorded at 800 MHz with $18 \times 44 \times 818$ complex points in t_1(^{13}CO),t_2(^{15}N),t_3(^{1}HN) (acquisition times of 8.5 ms, 19.0 ms, 64.0 ms in t_1,t_2,t_3). A total of 16 scans were obtained per FID with a relaxation delay of 1.5 seconds to give a net measuring time of 21 hours per spectrum. Reference intensities were measured from a 3D TROSY-HNCO spectrum recorded with a ten second relaxation delay, four scans and all other parameters as above. Exchange rate constants were extracted from a least-squares fit of normalized

† http://www.bmrb.wisc.edu

peak intensities to a magnetization build-up equation described elsewhere.[38]

Analysis of dipolar couplings and ^{13}CO chemical shift changes upon alignment

Alignment parameters, A_a, R, and the three Euler angles {α, β, γ}, were obtained by optimizing the agreement between the experimental dipolar couplings and the couplings predicted from the glyoxylate-bound MSG X-ray structure[4] using in-house software RDCA.[22,31] Predicted values are calculated from the coordinates of the 3D structure of MSG[4] using the following relationship:[12,25]

$$D_{ij} = D_{ij}^0 A_a S \left[(3\cos^2\theta - 1) + \frac{3}{2} R \sin^2\theta \cos 2\phi \right] \quad (4)$$

where $D_{ij}^0 = -(1/2\pi)(\mu_0/4\pi)\gamma_i\gamma_j\hbar\langle r_{ij}^{-3}\rangle$ is the dipolar interaction constant, r_{ij} is the distance between nuclei i and j, γ_i is the gyromagnetic ratio of nucleus i, S is the order parameter that reflects averaging due to fast local dynamics, and A_a and R are the axial and rhombic components of the alignment tensor, respectively. The polar angles {θ, ϕ} describe the orientation of the dipolar vector with respect to the alignment frame, while the Euler angles {α, β, γ} give the orientation of the principal axes of the alignment tensor with respect to the PDB frame. Errors in the alignment parameters were estimated on the basis of jackknife analyses where 20% of the data was removed from each of 100 iterations and by a Monte Carlo approach, using a standard error in dipolar coupling values of 3.2 Hz. The larger of the two sets of errors is reported for {A_a, R, α, β, γ} in the legend to Figure 3.

The change in chemical shift for a ^{13}CO spin upon alignment was calculated from the following relationship:[25,29]

$$\Delta\delta = 1/3 \sum_{i=x,y,z} \sum_{j=x,y,z} A_{jj} \cos^2\theta_{ij}\delta_{ii} \quad (5)$$

where θ_{ij} is the angle between the ii principal axis of the traceless CSA tensor (with principal components δ_{ii}) and the jj principal axis of the traceless molecular alignment tensor (with principal values A_{jj}). The following values were used for the ^{13}CO CSA tensor components: $\delta_{xx} = 73.33$ ppm, $\delta_{yy} = 7.33$ ppm and $\delta_{zz} = -80.66$ ppm with the z axis orthogonal to the peptide plane and the x axis forming an angle of 40° with respect to the CO–N bond (see Figure 1 of Choy *et al.*[31]); these values were not altered during calculation of the r.m.s.d between calculated and experimental ^{13}CO chemical shifts. In addition to the CSA dependent chemical shift offset there is an additional constant offset that derives from the fact that the frequency at which the spectrometer is locked changes with alignment. This is easily taken into account from the ^2H_2O splitting in the aligned sample, as described.[31]

Binding constants and line-shape analysis

Dissociation constants for the pyruvate–MSG and glyoxylate–MSG complexes were obtained from least-squares fitting of chemical shift changes as a function of total ligand concentration according to the relation:[53]

$$\delta_i = \frac{b - \sqrt{b^2 - 4 \times a \times c}}{2a} \quad (6)$$

with $a = (K_a/\delta_b) \times [P_t]$, $b = 1 + K_a([L_{ti}] + [P_t])$, and $c = \delta_b K_a[L_{ti}]$, where δ_i is the absolute change in chemical shift for each titration point, $[L_{ti}]$ is the total ligand concentration at each titration point, $[P_t]$ is the total protein concentration, $K_a = 1/K_d$ is the binding constant, and δ_b is the chemical shift of the resonance in question in the complex. K_d and δ_b were used as fitting parameters in this analysis.

Line-shape simulations of MSG spectra at different ligand concentration were performed separately in ^{1}HN and ^{15}N dimensions using software written for MATLAB v.6 (MathWorks Inc., MS). Analytical expressions for line-shapes in NMR spectra of exchanging systems commonly used to simulate two-site exchange[54,55] were used, with a pseudo-first-order on-rate, k_{on}[L]. The line intensities in a given dimension at each titration point were scaled using adjustable coefficients[42] to account for (i) possible line broadening in the other dimension and (ii) ligand-dependent efficiencies of INEPT-based magnetization transfers in the pulse sequence, as described in Results and Discussion. In each simulation the fitted parameters included k_{on} and the adjustable coefficients (equal to the number of simultaneously fitted titration points). The intrinsic transverse relaxation times were not used as free fitting parameters and were estimated as $1/(\pi \times LW)$, where LW is the peak line width (Hz) at half-height in a given dimension of the 2D TROSY-HSQC spectrum of the ligand-free protein.

Acknowledgements

This work was supported by a grant from the Canadian Institutes of Health Research to L.E.K. We thank Professor S. J. Remington (University of Oregon) for the gift of the plasmid used for MSG expression and for a number of valuable discussions during the course of this work, Professor Cheryl Arrowsmith (Ontario Cancer Institute) for kindly allowing us to carry out the protein expression and purification in her laboratory, Dr Nico Tjandra (NIH, Bethesda, MD) for the program to calculate dipolar couplings resulting from alignment due to magnetic susceptibility anisotropy, and Drs Oscar Millet, Martin Tollinger and Dmitry Korzhnev (University of Toronto) for assistance and helpful discussions. V.T. is a recipient of a Human Frontiers Postdoctoral Fellowship. L.E.K. holds a Canada Research Chair in Biochemistry.

References

1. Molina, I., Pellicer, M. T., Badia, J., Aguilar, J. & Baldoma, L. (1994). Molecular characterization of *Escherichia coli* malate synthase G. Differentiation with the malate synthase A isoenzyme. *Eur. J. Biochem.* **224**, 541–548.
2. Cornforth, J. W., Redmond, J. W., Eggerer, H., Buckel, W. & Gutschow, C. (1969). Asymmetric methyl groups, and the mechanism of malate synthase. *Nature*, **221**, 1212–1213.
3. Luthy, J., Retey, J. & Arigoni, D. (1969). Preparation and detection of chiral methyl groups. *Nature*, **221**, 1213–1215.

4. Howard, B. R., Endrizzi, J. A. & Remington, S. J. (2000). Crystal structure of *Escherichia coli* malate synthase G complexed with magnesium and glyoxylate at 2.0 Å resolution: mechanistic implications. *Biochemistry*, **39**, 3156–3168.
5. Schmid, G., Durchschlag, H., Biedermann, G., Eggerer, H. & Jaenicke, R. (1974). Molecular structure of malate synthase and structural changes upon ligand binding to the enzyme. *Biochem. Biophys. Res. Commun.* **58**, 419–426.
6. Beeckmans, S., Khan, A. S., Kanarek, L. & Van Driessche, E. (1994). Ligand binding to maize (Zea mays) malate synthase: a structural study. *Biochem. J.* **303**, 413–421.
7. Zipper, P. & Durchschlag, H. (1977). Small-angle X-ray studies on malate synthase from baker's yeast. *Biochem. Biophys. Res. Commun.* **75**, 394–400.
8. Larsen, T. M., Laughlin, L. T., Holden, H. M., Rayment, I. & Reed, G. H. (1994). Structure of rabbit muscle pyruvate kinase complexed with Mn2 + , K + , and pyruvate. *Biochemistry*, **33**, 6301–6309.
9. Larsen, T. M., Laughlin, L. T., Holden, H. M., Rayment, I. & Reed, G. H. (1997). Ligand-induced domain movement in pyruvate kinase: structure of the enzyme from rabbit muscle with Mg2 + , K + , and L-phospholactate at 2.7 Å resolution. *Arch. Biochem. Biophys.* **345**, 199–206.
10. Remington, S. J., Wiegand, G. & Huber, R. (1982). Crystallographic refinement and atomic models of two different forms of citrate synthase at 2.7 and 1.7 Å resolution. *J. Mol. Biol.* **158**, 111–152.
11. Tugarinov, V., Muhandiram, R., Ayed, A. & Kay, L. E. (2002). Four-dimensional NMR spectroscopy of a 723-residue protein: chemical shift assignments and secondary structure of malate synthase G. *J. Am. Chem. Soc.* **124**, 10025–10035.
12. Tjandra, N. & Bax, A. (1997). Direct measurement of distances and angles in biomolecules by NMR in a dilute liquid crystalline medium. *Science*, **278**, 1111–1114.
13. Hansen, M. R., Mueller, L. & Pardi, A. (1998). Tunable alignment of macromolecules by filamentous phage yields dipolar coupling interactions. *Nature Struct. Biol.* **5**, 1065–1074.
14. Clore, G. M., Starich, M. R. & Gronenborn, A. M. (1998). Measurement of residual dipolar couplings of macromolecules aligned in the nematic phase of a colloidal suspension of rod-shaped viruses. *J. Am. Chem. Soc.* **120**, 10571–10572.
15. Ottiger, M. & Bax, A. (1999). Bicelle-based liquid crystals for NMR-measurement of dipolar couplings at acidic and basic pH values. *J. Biomol. NMR*, **13**, 187–191.
16. Ruckert, M. & Otting, G. (2000). Alignment of biological macromolecules in novel nonionic liquid crystalline media for NMR experiments. *J. Am. Chem. Soc.* **122**, 7793–7797.
17. Ottiger, M., Delaglio, F. & Bax, A. (1998). Measurement of *J* and dipolar couplings from simplified two-dimensional NMR spectra. *J. Magn. Reson.* **131**, 373–378.
18. Yang, D., Venters, R. A., Mueller, G. A., Choy, W. Y. & Kay, L. E. (1999). TROSY-based HNCO pulse sequences for the measurement of $^{1}HN-^{15}N$, $^{15}N-^{13}CO$, $^{1}HN-^{13}CO$, $^{13}CO-^{13}C\alpha$ dipolar couplings in ^{15}N, ^{13}C, ^{2}H-labeled proteins. *J. Biomol. NMR*, **14**, 333–343.
19. Kontaxis, G., Clore, G. M. & Bax, A. (2000). Evaluation of cross-correlation effects and measurement of one-bond couplings in proteins with short transverse relaxation times. *J. Magn. Reson.* **143**, 184–196.
20. Permi, P. (2000). A set of HNCO-based experiments for measurement of residual dipolar couplings in ^{15}N, ^{13}C, (^{2}H)-labeled proteins. *J. Biomol. NMR*, **17**, 43–54.
21. Fischer, M. W., Losonczi, J. A., Weaver, J. L. & Prestegard, J. H. (1999). Domain orientation and dynamics in multidomain proteins from residual dipolar couplings. *Biochemistry*, **38**, 9013–9022.
22. Skrynnikov, N. R., Goto, N. K., Yang, D., Choy, W. Y., Tolman, J. R., Mueller, G. A. & Kay, L. E. (2000). Orienting domains in proteins using dipolar couplings measured by liquid-state NMR: differences in solution and crystal forms of maltodextrin binding protein loaded with β-cyclodextrin. *J. Mol. Biol.* **295**, 1265–1273.
23. Evenas, J., Tugarinov, V., Skrynnikov, N. R., Goto, N. K., Muhandiram, R. & Kay, L. E. (2001). Ligand-induced structural changes to maltodextrin-binding protein as studied by solution NMR spectroscopy. *J. Mol. Biol.* **309**, 961–974.
24. Pervushin, K., Riek, R., Wider, G. & Wüthrich, K. (1997). Attenuated T_2 relaxation by mutual cancellation of dipole–dipole coupling and chemical shift anisotropy indicates an avenue to NMR structures of very large biological macromolecules in solution. *Proc. Natl Acad. Sci. USA*, **94**, 12366–12371.
25. Bastiaan, E. W., MacLean, C., van Zijl, P. C. M. & Bothner-By, A. A. (1987). High resolution NMR of liquids and gases: effects of magnetic-field-induced molecular alignment. *Annu. Rep. NMR Spectrosc.* **9**, 3635–3677.
26. Tolman, J. R., Flanagan, J. M., Kennedy, M. A. & Prestegard, J. H. (1995). Nuclear magnetic dipole interactions in field-oriented proteins: information for structure determination in solution. *Proc. Natl Acad. Sci.* **92**, 9279–9283.
27. Tjandra, N., Grzesiek, S. & Bax, A. (1996). Magnetic field dependence of nitrogen-proton *J* splittings in ^{15}N enriched human ubiquitin resulting from relaxation interference and residual dipolar coupling. *J. Am. Chem. Soc.* **118**, 6264–6272.
28. Ottiger, M., Tjandra, N. & Bax, A. (1997). Magnetic field dependent amide ^{15}N chemical shifts in a protein–DNA complex resulting from magnetic ordering in solution. *J. Am. Chem. Soc.* **119**, 9825–9830.
29. Cornilescu, G., Marquardt, J., Ottiger, M. & Bax, A. (1998). Validation of protein structure from anisotropic carbonyl chemical shifts in a dilute liquid crystalline phase. *J. Am. Chem. Soc.* **120**, 6836–6837.
30. Boyd, J. & Redfield, C. (1999). Characterization of ^{15}N chemical shift anisotropy from orientation-dependent changes to ^{15}N chemical shifts in dilute bicelle solution. *J. Am. Chem. Soc.* **121**, 7441–7442.
31. Choy, W. Y., Tollinger, M., Mueller, G. A. & Kay, L. E. (2001). Direct structure refinement of high molecular weight proteins against residual dipolar couplings and carbonyl chemical shift changes upon alignment: an application to maltose binding protein. *J. Biomol. NMR*, **21**, 31–40.
32. Lipsitz, R. S. & Tjandra, N. (2001). Carbonyl CSA restraints from solution NMR for protein structure refinement. *J. Am. Chem. Soc.* **123**, 11065–11066.
33. Wu, Z., Tjandra, N. & Bax, A. (2001). ^{31}P chemical shift anisotropy as an aid in determining nucleic acid structure in liquid crystals. *J. Am. Chem. Soc.* **123**, 3617–3618.

34. Teng, Q., Iqbal, M. & Cross, T. A. (1992). Determination of the ^{13}C chemical shift and ^{14}N electric field gradient tensor orientations with respect to the molecular frame in a polypeptide. *J. Am. Chem. Soc.* **114**, 5312–5321.
35. Yang, D. & Kay, L. E. (1999). Improved ^{1}HN-detected triple resonance TROSY-based experiments. *J. Biomol. NMR*, **13**, 3–10.
36. Salzmann, M., Pervushin, K., Wider, G., Senn, H. & Wüthrich, K. (1998). TROSY in triple-resonance experiments: new perspectives for sequential NMR assignment of large proteins. *Proc. Natl Acad. Sci. USA*, **95**, 13585–13590.
37. Mulder, F. A. A., Schipper, D., Bott, R. & Boelens, R. (1999). Altered flexibility in the substrate-binding site of related natve and engineered high-alkaline *Bacillus subtilisins*. *J. Mol. Biol.* **292**, 111–123.
38. Hwang, T. L., van Zijl, P. C. & Mori, S. (1998). Accurate quantitation of water–amide proton exchange rates using the phase-modulated CLEAN chemical EXchange (CLEANEX-PM) approach with a Fast-HSQC (FHSQC) detection scheme. *J. Biomol. NMR*, **11**, 221–226.
39. Palmer, A. G., Kroenke, C. D. & Loria, J. P. (2001). NMR methods for quantifying microsecond-to-millisecond motions in biological macromolecules. *Methods Enzymol.* **339**, 204–238.
40. Sandstrom, J. (1982). *Dynamic NMR Spectroscopy*, Academic Press, New York.
41. Hensmann, M., Booker, G. W., Panayotou, G., Boyd, J., Linacre, J., Waterfield, M. & Campbell, I. D. (1994). Phosphopeptide binding to the N-terminal SH2 domain of the p85 alpha subunit of PI 3′-kinase: a heteronuclear NMR study. *Protein Sci.* **3**, 1020–1030.
42. Günther, U. L. & Schaffhausen, B. (2002). NMRKIN: simulating lineshapes from two-dimensional spectra of proteins upon ligand binding. *J. Biomol. NMR*, **22**, 201–209.
43. Fersht, A. (1985). *Enzyme Structure and Mechanism*, 2nd edit., Freeman, Co, New York.
44. Feher, V. A., Baldwin, E. P. & Dahlquist, F. W. (1996). Access of ligands to cavities within the core of a protein is rapid. *Nature Struct. Biol.* **3**, 516–521.
45. Prestegard, J. H. (1998). New techniques in structural NMR—anisotropic interactions. *Nature Struct. Biol. NMR supplement*, **5**, 517–522.
46. Zweckstetter, M. & Bax, A. (2001). Characterization of molecular alignment in aqueous suspensions of Pf1 bacteriophage. *J. Biomol. NMR*, **20**, 365–377.
47. Garrett, D. S., Powers, R., Gronenborn, A. M. & Clore, G. M. (1991). A common sense approach to peak picking in two-, three-, and four-dimensional spectra using automatic computer analysis of contour diagrams. *J. Magn. Reson.* **95**, 214–220.
48. Yang, D. & Kay, L. E. (1999). Improved lineshape and sensitivity in the HNCO-family of triple-resonance experiments. *J. Biomol. NMR*, **14**, 273–276.
49. Yang, D. & Kay, L. E. (1999). TROSY triple resonance four-dimensional NMR spectroscopy of a 46 ns tumbling protein. *J. Am. Chem. Soc.* **121**, 2571–2575.
50. Delaglio, F., Grzesiek, S., Vuister, G. W., Zhu, G., Pfeifer, J. & Bax, A. (1995). NMRPipe: a multidimensional spectral processing system based on UNIX pipes. *J. Biomol. NMR*, **6**, 277–293.
51. Johnson, B. A. & Blevins, R. A. (1994). NMRView: a computer program for the visualization and analysis of NMR data. *J. Biomol. NMR*, **4**, 603–614.
52. Farrow, N. A., Muhandiram, R., Singer, A. U., Pascal, S. M., Kay, C. M., Gish, G. *et al.* (1994). Backbone dynamics of a free and phosphopeptide-complexed src homology 2 domain studied by ^{15}N NMR relaxation. *Biochemistry*, **33**, 5984–6003.
53. Johnson, P. E., Tomme, P., Joshi, M. D. & McIntosh, L. P. (1996). Interaction of soluble cellooligosaccharides with the N-terminal cellulose-binding domain of Cellulomonas fimi CenC 2. NMR and ultraviolet absorption spectroscopy. *Biochemistry*, **35**, 13895–13906.
54. Huang, G. S. & Oas, T. G. (1995). Submillisecond folding of monomeric γ repressor. *Proc. Natl Acad. Sci. USA*, **92**, 6878–6882.
55. Burton, R. E., Busby, R. S. & Oas, T. G. (1998). ALASKA: a mathematica package for two-state kinetic analysis of protein folding reactions. *J. Biomol. NMR*, **11**, 355–359.
56. Koradi, R., Billeter, M. & Wüthrich, K. (1996). MOLMOL: a program for display and analysis of macromolecular structures. *J. Mol. Graph.* **14**, 51–55.

Edited by P. Wright

(Received 5 November 2002; received in revised form 31 January 2003; accepted 31 January 2003)